



*Citation for published version:*

Bowen, C & Zhang, R 2018, 'Intrinsic Tuning of Poly(styrene–butadiene–styrene)-Based Self-Healing Dielectric Elastomer Actuators with Enhanced Electromechanical Properties', ACS Applied Materials and Interfaces, vol. 10, pp. 38438-38448. <https://doi.org/10.1021/acsami.8b13785>

*DOI:*

[10.1021/acsami.8b13785](https://doi.org/10.1021/acsami.8b13785)

*Publication date:*

2018

*Document Version*

Peer reviewed version

[Link to publication](#)

This document is the Accepted Manuscript version of a Published Work that appeared in final form in Applied Materials and Interfaces, copyright (C) American Chemical Society after peer review and technical editing by the publisher. To access the final edited and published work see: <https://pubs.acs.org/doi/pdf/10.1021/acsami.8b13785>

## University of Bath

### General rights

Copyright and moral rights for the publications made accessible in the public portal are retained by the authors and/or other copyright owners and it is a condition of accessing publications that users recognise and abide by the legal requirements associated with these rights.

### Take down policy

If you believe that this document breaches copyright please contact us providing details, and we will remove access to the work immediately and investigate your claim.

# Intrinsic Tuning of Poly(styrene-butadiene-styrene) (SBS) Based Self-healing Dielectric Elastomer Actuators with Enhanced Electromechanical Properties

*Christopher Ellingford, Runan Zhang, Alan M. Wemyss, Christopher Bowen, Tony McNally,  
Łukasz Figiel, Chaoying Wan\**

Christopher Ellingford, Prof. Tony McNally, Dr. Łukasz Figiel, Dr. Chaoying Wan\*,

International Institute for Nanocomposites Manufacturing (IINM), WMG, University of  
Warwick, CV4 7AL, UK

*\*Email: Chaoying.wan@warwick.ac.uk*

Runan Zhang, Prof. Christopher Bowen

Department of Mechanical Engineering, University of Bath, BA2 2ET, UK

Dr. Alan Wemyss

Department of Chemistry, University of Warwick, CV4 7AL, UK

Keywords: self-healing, dielectric elastomer, chemical modification, actuation, electrical  
breakdown recovery

## Abstract

The electromechanical properties of a thermoplastic styrene-butadiene-styrene (SBS) dielectric elastomer was intrinsically tuned by chemical grafting with polar organic groups. Methyl thioglycolate (MG) reacted with the butadiene block via a one-step thiol-ene 'click' reaction under UV at 25°C. The MG grafting ratio reached 98.5 mol% (with respect to the butadiene alkenes present) within 20 minutes and increased the relative permittivity to 11.4 at 10<sup>3</sup> Hz, with a low  $\tan \delta$ . The actuation strain of the MG grafted SBS dielectric elastomer actuator was ten times larger than the SBS-based actuator, and the actuation force was four times greater than SBS. The MG grafted SBS demonstrated an ability to achieve both mechanical and electrical self-healing. The electrical breakdown strength recovered to 15% of its original value, and the strength and elongation at break recovered by 25% and 21%, respectively, after three days. Self-healing was explained by the introduction of polar MG groups that reduce viscous loss and strain relaxation. The weak CH/ $\pi$  bonds through the partially charged ( $\delta^+$ ) groups adjacent to the ester of MG and the  $\delta^-$  centre of styrene enable polymer chains to reunite and recover properties. Intrinsic tuning can therefore enhance the electromechanical properties of dielectric elastomers and provides new actuator materials with self-healing of mechanical and dielectric properties.

## 1. Introduction

Smart electroactive polymers are able to change their shape and size under applied electric fields, and operate through ionic or electronic actuation mechanisms.. Dielectric elastomers are a class of electronically active polymers<sup>1</sup> which exhibit strains typically up to 400%, fast response times under an applied electric field and can transduce electrical energy into mechanical energy (actuation) or *vice versa* for energy harvesting applications.<sup>2,3</sup>

Dielectric elastomers typically exhibit a low permittivity, which limits performance for actuator and energy harvesting applications due to a low maximum theoretical energy density, given by Eq.1:

$$U_e = 0.5\varepsilon_r\varepsilon_0E_b^2 \quad (1)$$

Where  $U_e$  is the theoretical energy density,  $\varepsilon_r$  the relative permittivity,  $\varepsilon_0$  the permittivity of free space and  $E_b$  the breakdown strength. The high breakdown strength and low stiffness of dielectric elastomers, in comparison to piezoelectric ceramic materials, are of interest for use in actuation and energy generation applications. An increase of their relative permittivity has the potential to increase performance significantly, as indicated in Eq.1.

Extensive research has focussed on improving the relative permittivity of dielectric elastomers, either *extrinsically* through the addition of fillers or *intrinsically* through chemical modification. The extrinsic approach of incorporating ceramic fillers, such as BaTiO<sub>3</sub><sup>4,5</sup> or electrically conducting metallic or carbon based nanomaterials<sup>6,7</sup> has the advantage of using materials with a high relative permittivity to increase the effective permittivity of the composites. However, the enhancement in the relative permittivity of such materials is limited by the poor compatibility between the filler surface and the polymer matrix, and is often at the expense of a reduced breakdown strength,<sup>1,8</sup> reduced mechanical properties<sup>9</sup> and a large dielectric loss<sup>9</sup> due to interfacial defects.<sup>10</sup>

Intrinsic chemical modification of dielectric elastomers is achieved through chemically grafting polar groups to elastomers to increase the atomic polarisation by increasing the dipole moment across the polymer chain.<sup>11-13</sup> Chemical modification is advantageous compared to extrinsic modification methods as it can maintain a low dielectric loss and a high breakdown strength due to the formation of a homogeneous polymer structure. The deformable nature of the elastomers can also be maintained after modification.<sup>1</sup>

Small polar groups including allyl cyanide,<sup>14</sup> 3-mercaptopropionitrile<sup>15-16</sup> and 2-(methylsulfonyl)-ethanethiol,<sup>17</sup> and liquid crystal<sup>18-19</sup> have been grafted to various polymer structures resulting in an

increase in their relative permittivity up to 22.7.<sup>17</sup> Grafting conducting polyaniline to polyurethane through a copper phthalocyanine ring resulted in a large increase in relative permittivity to 105.<sup>20</sup>

To further enhance the electrical breakdown strength, a novel approach is to enable the elastomer to self-heal either electrically or mechanically, so that the material can sustain large numbers of operational cycles under high electric field conditions without experiencing breakdown.<sup>1, 21-22</sup> Self-healing is normally achieved through non-covalent interactions such as hydrogen bonding,<sup>23</sup>  $\pi$ - $\pi$  stacking and interpenetrating polymer networks.<sup>22</sup> One example of a self-healing actuator has used an iron catalyst incorporated into poly(dimethylsiloxane) to act as the crosslinker. After mechanically damaging the material with a hole and leaving it for 72 hours to heal, the material showed no electrical breakdown at the damaged site until the electric field was 188 kV cm<sup>-1</sup>.<sup>24</sup>

In this paper, poly(styrene-butadiene-styrene) (SBS) block copolymer (Vector 8505A) is chemically grafted with methyl thioglycolate (MG) through a thiol-ene click chemistry. The SBS material was specifically selected for this study due to its high strain at break (over 800%), high breakdown strength ( $\sim 65 \text{ V } \mu\text{m}^{-1}$ )<sup>25</sup>, and ease of processing where the available alkene groups on the butadiene block that can be readily modified via a thiol-ene click chemistry. The attachment of polar groups has further increased the tensile strain, reduced the viscous loss, enhanced relative permittivity without increasing the dielectric loss, which leads to a significant enhanced electromechanical properties and actuation performance of the modified SBS. In addition, we demonstrate that the modified SBS exhibits rapid self-healing behaviour, which provides the potential to increase the lifetime of the material in actuation and energy generation applications and enable the material to be reused in the event of failure. The self-healing mechanism is analysed from the perspective of the macromolecular interactions. This work will inspire further research into the area of self-healing dielectric elastomers to develop materials

which not only have excellent mechanical and electrical properties, but also excellent cycle lifetimes and endurance.

## 2. Experimental

### 2.1. Materials

Styrene-butadiene-styrene block copolymer (SBS, Vector 8508A) was purchased from Dexco. Tetrahydrofuran (THF, GPR Reactapur, 99.9%) was purchased from VWR, UK. Hexane (for HPLC >95%), chloroform-*d* (99.8%), 2,2-dimethoxy-2-phenylacetophenone (DMPA, 99%) and methyl thioglycolate (95%) were purchased from Sigma-Aldrich, UK. Carbon black grease was purchased from MG Chemicals, UK to act as a compliant electrode for actuator studies.

### 2.2. Synthesis

In a typical synthesis, 10 g SBS was dissolved in 90 g of THF. Following this, 0.2 g of DMPA and 46.9 mL (4× molar excess relative to the butadiene block of SBS) of methyl thioglycolate (MG) was added to the solution. The solution was then irradiated with UV light @ 365 nm with 25% intensity (50 W) using an OmniCure Series 2000 200 W UV lamp for 5 to 20 minutes. The resulting modified SBS was purified by precipitation in hexane and dried in a vacuum oven overnight at 60 °C. The mass of the resulting product was 21.3 g (98.5% grafting). <sup>1</sup>H NMR (400 MHz, CDCl<sub>3</sub>): δ = 7.07 (br, 3 H, H<sub>benzene</sub>), 6.53 (br, 2 H, H<sub>benzene</sub>), 5.39 (br, 4 H, -HC=CH- and HC=CH<sub>2</sub>), 3.73 (s, 3 H, COOCH<sub>3</sub>), 3.23 (s, 2 H, OOC-CH<sub>2</sub>-S), 2.75 (br, 1 H, (CH<sub>2</sub>)<sub>2</sub>CHS), 2.64 (br, 2 H, H<sub>2</sub>CCH<sub>2</sub>S), 1.73 (br, 2 H, H<sub>2</sub>C-CH<sub>2</sub>-CH), 1.55 (br, 6 H, (-H<sub>2</sub>C)<sub>2</sub>CH<sub>2</sub>, -HCCH<sub>2</sub>CH<sub>2</sub>- and (-HC)<sub>2</sub>CH<sub>2</sub>), 1.43 (br, 2 H, -HCCH<sub>2</sub>CH<sub>2</sub>), 1.26 (br, 1 H, (H<sub>2</sub>C)<sub>3</sub>CH) ppm. FT-IR (cm<sup>-1</sup>): 2927, 1729, 1435, 1272, 1128, 1007, 757. The methyl thioglycolate modified SBS with different graft molar ratios is denoted as MGSBS (x%), i.e., MGSBS (53.7%) @5 mins UV, MGSBS (68.3%) @10 mins UV and MGSBS (98.5%) @20 mins UV.

### 2.3. Characterisation

SBS and MGSBS were characterised by  $^1\text{H}$  NMR, all spectra were recorded using a Bruker Avance III HD 400 MHz spectrometer. Chemical shifts were internally referenced to TMS using  $\text{CDCl}_3$ . Spectra were processed using ACD/NMR processor version 12.01 (ACD/Labs). Gel Permeation Chromatography (GPC) was carried out using an Agilent 390-MDS with two PLgel Mixed-C columns and THF with 2% TEA + 0.01% BHT as an eluent and analysed using Agilent GPC/SEC software.

Tensile testing was performed using a Shimadzu Autograph AGS-X tester with samples conforming to ASTM-D638-14 type V. The extension rate was  $50 \text{ mm min}^{-1}$  (strain rate =  $10.95\% \text{ s}^{-1}$ ) with a 10 kN load cell and tests were carried out at room temperature. Stress relaxation testing was investigated by stretching the tensile specimens to 100% elongation at  $50 \text{ mm min}^{-1}$  and holding the samples at constant strain until the stress reached equilibrium. Cyclic stress softening was performed by elongating specimens to 100%, 300% and 500% elongation and back to 0% under a controlled strain rate of  $50 \text{ mm min}^{-1}$  for 5 cycles. Fourier transform infrared spectroscopy (FT-IR) using a Bruker Tensor 27 at a resolution of  $4 \text{ cm}^{-1}$  with 32 scans. Raman Spectra were recorded using a Renishaw inVia Reflex Raman Microscope with a 532 nm diode-pumped solid-state laser. UV-Vis was performed using an Agilent Cary 60 photospectrometer between 200 nm and 800 nm. Samples were dissolved in DCM to a concentration of  $1 \times 10^{-5} \text{ mol dm}^{-3}$  for the solution state. Solid state UV was performed on compression moulded thin films of 0.5 mm thickness. Dynamic Mechanical Thermal Analysis (DMTA) was performed on samples  $5.0 \text{ mm} \times 5.0 \text{ mm} \times 2.3 \text{ mm}$  in single cantilever mode with a  $50 \text{ }\mu\text{m}$  amplitude and a frequency of 1 Hz between  $-120 \text{ }^\circ\text{C}$  and  $135 \text{ }^\circ\text{C}$ . Small Angle X-ray Scattering (SAXS) was carried out using a Xenocs Xeuss 2.0 SAXS system equipped with both a 1-D and 2-D detector. AFM was imaged using a Bruker Dimension Icon in Peakforce QNM mode with Scanasyt-Air tips using tapping mode at a scan rate of 0.2 Hz.

Impedance spectroscopy measurements were carried out using a Princeton Applied Research Parastat MC with a PMC-2000 card and a two-point probe between  $10^0 \sim 10^6 \text{ Hz}$  on thin films of

thickness between 100~200  $\mu\text{m}$  that were formed by compression moulding using a Rondol manual hot press at 190  $^{\circ}\text{C}$  and 5 kN of force.

#### 2.4 Dielectric elastomer actuation

To demonstrate the actuation function, the MGSBS and SBS films were coated with a compliant electrode based on a carbon black grease from MG Chemicals to enable the two types of elastomers to be actuated under driving voltages (in kV). The following configurations were arranged: (i) Dielectric elastomer actuation in strain: The MGSBS and SBS were cut into samples of area 30 mm  $\times$  30 mm and pre-strained by 33.33% in planar directions and clamped onto the rigid frame as shown in Figure S1a. Carbon black grease was applied to form a circular electrode region of diameter 15 mm from the centre. The actuation was driven by voltages of 3, 4 and 5 kV, and the pre-strained state and the actuated state of the samples were recorded by a camera to allow estimation of the voltage-induced planar deformation. To ensure the actuation reached a steady state, the actuation state was set to be 5 seconds after switching on the high voltage power supply. (ii) actuation in force: The MGSBS and the SBS were cut into samples of area 40 mm  $\times$  40 mm with a rectangular electrode region of area 20 mm  $\times$  20 mm defined prior to pre-strain. The samples were then pre-strained by 20% in the direction of actuation, fixed to the test rig on the top and mounted onto a load cell on the bottom as shown in Figure S1b. The load cell was customized to measure small forces up to 5 N. The high voltages were applied to the samples in a sequence that lasted 60 seconds, as shown in Figure S1c. The force was measured by the load cell throughout. A high voltage (HV) generator, based on a HV DC-DC converter (module 15A24 from PPMTM), was used to amplify the input voltage (0-5 V) to the voltage output (0-15 kV). In the second set of experiments, the actual voltage output was also measured using a built-in channel from the HV module.

### 3. Results and Discussion



### 3.1. Chemical Modification of SBS

MGSBS was synthesised *via* a thiol-ene click reaction in air and at room temperature, the structures were verified *via*  $^1\text{H}$  NMR, FT-IR and GPC. MG was kept in a three or four times molar excess with respect to the butadiene section of SBS, and no gelation was detected during the reaction as characterised by  $^1\text{H}$  NMR.

$^1\text{H}$  NMR and FT-IR spectra of the resultant MGSBS are given in Figure 1a and b. In Figure 1a the characteristic  $\text{CH}_2$  and  $\text{CH}_3$  peaks in  $^1\text{H}$  NMR were observed at 3.23 and 3.73 ppm, respectively, which were absent in the  $^1\text{H}$  NMR of SBS, as seen in Figure S2. The reduction in the alkene peaks of the butadiene block at 5.39 and 4.98 ppm is apparent as the grafting ratio increases, indicating that the reaction of methyl thioglycolate and the vinyl groups of butadiene had taken place. Furthermore, FT-IR confirmed the presence of a C=O stretch for an ester group at  $1729\text{ cm}^{-1}$  and two C-O stretches at  $1272$  and  $1020\text{ cm}^{-1}$  to indicate the successful grafting of methyl thioglycolate onto the SBS backbone.  $^1\text{H}$  NMR was used to determine the grafting efficiency of the reaction at different UV exposure times. Increasing the UV light exposure time from 5 to 20 minutes resulted in increasing the grafting ratio of MG to SBS from 53.7% up to 98.5%, with respect to the butadiene block.

The number average molecular weight ( $M_n=86158\text{ g mol}^{-1}$ ) and polydispersity index (PDI=1.17) of SBS chains become  $79417\text{ g mol}^{-1}$  and 2.57, respectively after grafting of 98.5% of methyl thioglycolate, indicating the UV initiated reaction caused some polymer chain scission. An increase in weight average molecular weight ( $M_w$ ) from  $100768\text{ g mol}^{-1}$  to  $203883\text{ g mol}^{-1}$  further confirmed the successful grafting of methyl thioglycolate to SBS.

### 3.2. Mechanical and electrical properties of methyl thioglycolate modified SBS

The equations of state for an ideal dielectric elastomer actuator can be expressed in Eq.2,<sup>26</sup>

$$\begin{aligned}\sigma_1 + \varepsilon E^2 &= \lambda_1 \frac{\partial W(\lambda_1, \lambda_2)}{\partial \lambda_1} \\ \sigma_2 + \varepsilon E^2 &= \lambda_2 \frac{\partial W(\lambda_1, \lambda_2)}{\partial \lambda_2}\end{aligned}\quad (2)$$

where  $\sigma_{1,2}$  are the applied stresses in planar directions,  $\lambda_{1,2}$  the stretches due to mechanical in planar directions,  $\varepsilon$  the permittivity of the dielectric elastomer ( $\varepsilon = \varepsilon_r \varepsilon_0$ ),  $E$  the applied electric field and  $W(\lambda_1, \lambda_2)$  the Helmholtz free energy density. By comparing the un-actuated ( $E = 0$ ) and actuated states, actuation stresses in planar directions,  $\Delta\sigma_{1,2}$ , correlate to the Maxwell pressure,  $\varepsilon E^2$ , as expressed in Eq.3,

$$\Delta\sigma_{1,2} \propto \varepsilon E^2 \quad (3)$$

For a dielectric elastomer actuator with equal bi-axial pre-strains, as in the actuation in strain experiment, the actuation strains in radius and area,  $\Delta s_r$  and  $\Delta s_a$ , correlate to the Maxwell pressure,  $\varepsilon E^2$ , and the elasticity modulus of the elastomer,  $Y$ , as shown in Eq.4.

$$\begin{aligned} s_r &\propto \varepsilon E^2, \frac{1}{Y} \\ s_a &= s_r^2 \end{aligned} \quad (4)$$

This indicates for actuation a high permittivity, high breakdown strength and low elasticity modulus are desirable, and the mechanical and electrical properties will now be described.

The mechanical properties of SBS and MGSBS are shown in Figure 2. After grafting of 98.5% of methyl thioglycolate, the tensile strength and elongation at break of SBS decreased from 9.00 MPa and 857%, to 3.13 MPa and 569%, respectively. The Young's modulus of SBS was significantly reduced from 51.7 MPa to 2.87 MPa, which will benefit the actuation function of dielectric elastomers, and will be discussed in the following sections.

The effects of grafting polar groups on the mechanical behaviour was examined by stress relaxation and cyclic stress softening experiments. The cyclic stress softening testing of SBS and MGSBS is shown in Figure 2b and c. In Figure 2b, SBS showed large viscous losses within the samples after five cycles regardless of whether the sample was elongated 100%, 300% or 500%. In comparison, Figure 2c shows that for MGSBS (98.5%) the viscous losses are very low for 100% and 300% elongation and are only observed in significant quantities for 500% elongation.

In fact, increasing the grafting of methyl thioglycolate results in a reduction in the viscous losses exhibited by the material at strains of 100% to 500%, as shown in Figure 2d.

The stress-relaxation of SBS and MGSBS were evaluated when subjected to a fixed 100% elongation until they reached equilibrium. As shown in Figure 3, MGSBS (98.5%) reached equilibrium after 10 minutes and the stress only decreased by 22%. This shows that its stronger intermolecular interactions prevent the polymer chains slipping and thus compensate the effect of reduced chain entanglement observed with MGSBS (53.7%). The reduced relaxation of MGSBS (98.5%) will also be of benefit for actuation to maintain a constant force or displacement.

The electrical properties of SBS and MGSBS were characterised by impedance spectroscopy. As shown in Figure 4, the initial unmodified SBS has a relative permittivity of 2.8, and AC conductivity of  $1 \times 10^9 \text{ S m}^{-1}$  at  $10^3 \text{ Hz}$ , showing the highly insulating nature of SBS. The grafting of 98.5 % methyl thioglycolate to SBS results in an increase in relative permittivity up to 11.4 at  $10^3 \text{ Hz}$ , close to that of the piezoelectric poly(vinylidene fluoride).<sup>27</sup> While the electrical  $\tan \delta$  remains similar to SBS at  $9 \times 10^{-3}$  for  $10^3 \text{ Hz}$  (where  $\tan \delta = \frac{\text{dielectric loss}}{\text{relative permittivity}}$ ), as seen in Figure 4b. Furthermore, the phase angle of both SBS and MGSBS remains at  $-90^\circ$ , see Figure S3, demonstrating the insulating nature of both elastomers.

The relative permittivity enhancement of the material is higher than that reported for chemical modification of SBS using an analogous polar group, thioglycolic acid, which was 7.2 at  $10^3 \text{ Hz}$ . Other examples in the literature include grafting 3-mercaptopropionitrile and 2-(methylsulfonyl)-ethanethiol to polydimethylsiloxane, which increased the relative permittivity to 18.4 and 22.7 respectively.<sup>15, 17</sup> However, these elastomers had dielectric losses several orders of magnitude higher than reported in this work, reducing their energy transduction efficiency.

In summary, the grafting of MG group of 98% to SBS has reduced the Young's modulus by 94%, reduced the viscous loss by up to 80% at 300% elongation, while enhancing the relative permittivity from 2.8 to 11.4, without increasing the dielectric loss. These results have directed

the MGSBS to a novel dielectric actuation material, and this is now demonstrated by valuation of SBS and MGSBS based actuators.

### 3.3. Dielectric elastomer actuation of SBS and MGSBS

Figure 5 shows that the MGSBS-based dielectric elastomer actuator generates 10 times larger actuation strain than the SBS-based DEA. The actuation strain was evaluated between the state with no electric field and the steady state after 5 seconds of applied electric field. Under an electric field of  $250 \text{ kV cm}^{-1}$ , the actuation strain in the MGSBS was measured to be 13% radially and 17% in area. The actuation strain of the SBS under the same electric field could not be obtained because electrical breakdown occurred in the electrode region immediately after the voltage application. Instead, the actuation strain of SBS was recorded at the lower field of  $200 \text{ kV cm}^{-1}$ . The actuation strains were measured to be only 1.2% radially and 1.4% in area. Three reasons for the outstanding actuation performance of the MGSBS compared with the SBS are

(i) its lower elastic modulus that results larger material deformation under the same Maxwell pressure, as discussed in section 3.2, Figure 2.

(ii) its higher relative permittivity (11.4) that generates larger Maxwell pressure under the same driving voltage (i.e. larger  $s_r$  and  $s_a$  according to Eq.4), as discussed in section 3.2, Figure 4.

(iii) its higher dielectric strength that allows higher driving voltage (i.e. larger  $\sigma_1$ ,  $s_r$  and  $s_a$  according to Eq.3 and 4).

Figure 5 shows the experimental results for dielectric elastomer actuation in force. Constant voltages were applied on the MGSBS-based and SBS-based actuators for 5 seconds from 3 kV ( $150 \text{ kV cm}^{-1}$ ) to 8 kV ( $400 \text{ kV cm}^{-1}$ ). Unlike the previous experiments, no electrical breakdown occurred for both materials since samples are pre-strained to a lower degree (20% in one direction compared with the equal-biaxial pre-strain of 33% in two directions), and are therefore thicker and have higher breakdown voltages. In this experiment, actuation force was defined as

the net force between the un-actuated state and the actuated state (5 seconds after voltage application). At an applied electric field of  $400 \text{ kV cm}^{-1}$ , the MGSBS generates an actuation force of  $0.12 \text{ N}$ , which is four times higher than the actuation force from the SBS ( $0.03 \text{ N}$ ). Unlike the measured the actuation strain, the actuation force is independent of the elastic modulus of the material and depends only on the Maxwell pressure (i.e. the relative permittivity of the material). The difference in actuation forces between the MGSBS and the SBS therefore, according to Eq.3, agrees well with the results of the improvement in dielectric properties, as in Figure 4.

### 3.4 Self-healing of methyl thioglycolate modified SBS

#### 3.4.1 Self-healing after mechanical breakdown

The MGSBS with a grafting ratio of  $98.5\%$  exhibited an unexpected, yet remarkable, ability to rapidly recover some of its mechanical properties upon reattaching two pieces of cut polymer; this was achieved simply by pushing two pieces together at room temperature without using any other external stimulus. This self-healing behaviour was observed for MGSBS at the higher grafting levels of  $68.3\%$  and  $98.5\%$ , but not for SBS or MGSBS at a lower grafting of  $53.7\%$ .

The extent of self-healing recovery for MGSBS ( $68.3\%$ ) and MGSBS ( $98.5\%$ ) was investigated for varying time periods at room temperature (thermostatically controlled to  $20^\circ\text{C}$ ) to determine how the tensile strength and elongation at break recovered over time. As shown in Figures S4a and S4b, a maximum tensile strength recovery of  $25.4\%$  ( $0.80 \text{ MPa}$ ) and an elongation at break recovery of  $20.9\%$  ( $116.6\%$  strain) were reached after three days ( $4320$  minutes). In comparison, the tensile strength recovery and elongation at break recovery was less than  $5\%$  for MGSBS ( $68.3\%$ ).

The temperature dependency of self-healing was investigated at  $37^\circ\text{C}$  for up to three days. For samples of MGSBS ( $98.5\%$ ) healed at  $37^\circ\text{C}$ , the tensile strength and elongation at break rapidly recovered to similar levels as those healed at room temperature, Figure S5. However, subsequent time intervals revealed the samples reached a maximum tensile recovery of  $17.0\%$  ( $0.5 \text{ MPa}$ ) and elongation at break recovery of  $13.3\%$  ( $70\%$  strain), demonstrating a highly temperature

sensitive nature. This suggests that the self-healing property is a result of weak intermolecular interactions that can be easily overcome, which provides further scope for developing high self-healing elastomers.

Furthermore, the potential reusability of the material through multiple self-healing cycles was investigated by using the same samples for all self-healing experiments. Figure 6 shows that after multiple self-healing cycles, the samples had a tensile strength recovery of 17.7% (0.56 MPa) and elongation at break recovery of 18.9% (105% strain) after three days. This demonstrates that the MGSBS can be self-healed multiple times without a major degradation of the self-healing ability.

#### 3.4.2 Self-healing under low electric field

While mechanical self-healing is of interest, the potential for healing after electric breakdown is of interest in dielectric elastomers due to the high operating electric fields. Figure 7 compares the AC conductivity, capacitance and phase angle of MGSBS (98.5%) (i) prior to breakdown, (ii) after breakdown, and (iii) 24 hours after breakdown. Prior to breakdown, MGSBS (98.5%) exhibits a low AC conductivity ( $< 1 \times 10^{-9} \text{ S m}^{-1}$ ), and it is frequency independent at low frequencies ( $< 1 \text{ kHz}$ ) and frequency dependent at high frequencies ( $> 1 \text{ kHz}$ ); this is often termed as the Universal Dielectric Response of many insulating materials including polymers.<sup>28</sup> Figure 7b shows that the capacitance of MGSBS (98.5%) is frequency independent for the frequency range studied, indicating a capacitive response due to the low conductivity of the material. The capacitive response can be observed in the phase angle, Figure 7c, where the phase angle is  $-90^\circ$  above 100 Hz, since in a capacitive material AC current lags AC voltage by  $90^\circ$ . At low frequencies, the phase angle approaches  $0^\circ$  due to the presence of a small conductivity in the material.

MGSBS (98.5%) was then subjected to dielectric breakdown. A high voltage of 8.5 kV (corresponding to  $200 \text{ kV cm}^{-1}$ ) was applied on the electrode region until electrical breakdown was detected in voltage monitoring channel of high voltage power supply. The voltage

application was then switched off immediately to stop the failure from further propagation. Electrical breakdown of the material leads to a formation of a pinhole, with a diameter of approximately 100  $\mu\text{m}$ . This is from thermal runaway due to localised Joule heating in the sample. Joule heating increases the electrical conductivity in those locations, causing further localised heating until breakdown of the material.<sup>29</sup>

After dielectric breakdown, the frequency dependency properties change significantly due to the electrical short circuit formed by the pinhole and a conductive path through the thickness of MGSBS (98.5%); for example, caused by carbon formation during breakdown. The AC conductivity increased significantly compared to before breakdown, Figure 7a, and is now frequency independent, typical of a pure conductor. This is also observed in the phase angle, which is close to  $0^\circ$  across the entire frequency range, because current and voltage are in phase for a conductor. The capacitance also increased significantly, which is common in materials dominated by conductivity.<sup>30</sup>

After a period of 24 hours, the frequency dependency properties are more similar to MGSBS (98.5%) before breakdown, where the AC conductivity, capacitance and phase angle indicate a capacitor behaviour of the healed MGSBS at the low electric fields ( $25 \text{ V cm}^{-1}$ ).

### 3.4.3 Self-healing under high electric field

Figure S6 shows the polarisation – electric field response of MGSBS (98.5%) for applied voltages up to 4 kV across a sample of approximately 400  $\mu\text{m}$ ; which corresponds to an electric field of  $100 \text{ kV cm}^{-1}$ . The polarisation – electric field is linear, since the MGSBS (98.5%) is capacitive and the constant gradient with field indicates that the permittivity is insensitive to applied electric field. To achieve electrical breakdown, a higher potential difference was required ( $\sim 8.5 \text{ kV}$ ), which corresponds to an electric field of  $200 \text{ kV cm}^{-1}$ . After 24 hours, the low field measurements, Figure 7, indicated healing had taken place; however, it is important to assess the response of healed MGSBS (98.5%) to higher electric fields which are typical of operation. The healed material after 24 hours could survive electric fields of  $12.5 \text{ kV cm}^{-1}$ , which is 6% of the initial breakdown strength. This initially modest healing may be the result of the healed material

containing electrically conductive regions, such as carbon, which can act as an electric field concentration to limit the amount of healing possible. The application of small mechanical compression to the damaged pinhole region enhanced healing and led to an improvement of the maximum applied electric field after 24 hours to 1.25 kV (31 kV cm<sup>-1</sup>), which is 15% of the original breakdown strength and similar to the mechanical property recovery (10-25%).

#### 3.4.4 Self-healing mechanism of MGSBS upon mechanical or electrical breakdown

To understand the electrical and mechanical self-healing behaviour of MGSBS, the microstructure evolution of the elastomers was considered. Firstly, as characterised by dynamic mechanical thermal analysis (DMTA), there are two steps in the storage modulus for SBS, Figure 8a, corresponding to the two glass transition temperatures ( $T_g$ 's) of the two phases –the polybutadiene block and the polystyrene block. Below  $T_g$ , the storage modulus for MGSBS (98.5%) is higher than SBS, reflecting a stronger intermolecular interaction among the MGSBS polymer chains than SBS, making the modified elastomer more rigid. For MGSBS (98.5%) there is a single strong peak for the glass transition temperature and several small peaks in the polybutadiene glass transition region due to the polymer chains that have been affected by chain scission or have a lower grafting of methyl thioglycolate. From the mechanical  $\tan \delta$  results in Figure 8b, the  $T_g$ 's occur as a sharp peak at -83 °C for polybutadiene and a broad peak at 97 °C for the polystyrene block. In comparison, MGSBS (98.5%) has only one strong decrease in the storage modulus, resulting in a  $T_g$  of -22 °C. The single transition temperature implies that the grafting of methyl thioglycolate groups has made the two polymer phases compatible.

The macromolecular interaction of MGSBS was further characterised by UV-vis spectroscopy. Both SBS and MGSBS (98.5%) in the solution state in dichloromethane (DCM) and in the solid state were compared, as shown in Figure S7 and Figure 8c respectively. In DCM, clear peaks for the  $\pi$ - $\pi^*$  transitions from free styrene and  $\pi$ -stacking styrene groups are clearly visible for both SBS and MGSBS. However, the  $\pi$ - $\pi^*$  transition for free styrene blue shifts by 15 nm to 247 nm because of the chemical modification. This implies that chemical modification with methyl



thioglycolate in the butadiene section results in an interaction with the styrene block of the polymer, at least in the solution state. In the solid-state UV-vis spectra in Figure 8c, the  $\pi$ - $\pi^*$  transition for  $\pi$ -stacking styrene had dramatically increased in its relative intensity to the free styrene transition, when compared to the spectra recorded in the solution state. This peak in MGSBS however was blue-shifted 20 nm compared to SBS. In addition, the free styrene  $\pi$ - $\pi^*$  transition peak is also blue-shifted in the solid material from 266 nm to 248 nm. This blue shift indicates that there is an increase in the transition energy for the styrene groups because of weak hydrogen bonding interactions with the aromatic electron density.<sup>31</sup> The peak at 205 nm is the transition from the alkenes on the butadiene block, which is not seen after chemical modification.<sup>32</sup>

Understanding the nature of self-healing was further explored through FT-IR and Raman spectroscopy. Shifts in the wavenumbers of peaks compared to the starting materials, or as grafting increases, implies that a change of environment is taking place and provides an insight into the interactions involved. In both FT-IR and Raman, Figure 1b and Figure 8d, the main peak shifts occur through C-O, C=O and C-C bonds on increasing the grafting concentration of methyl thioglycolate. In FT-IR, a 6  $\text{cm}^{-1}$  and 13  $\text{cm}^{-1}$  red shift was observed for both C-O bonds on methyl thioglycolate and also a 4  $\text{cm}^{-1}$  red shift for the C=O on the ester. Likewise, a 2  $\text{cm}^{-1}$  red shift was also observed for the C-C aromatic bond of styrene.

A 2  $\text{cm}^{-1}$  shift is normally attributed to variance in the equipment, however, in this case the same 2  $\text{cm}^{-1}$  drop for the C-C aromatic bond is also observed in the Raman spectrum. This indicates that the C-C bonds have become slightly elongated. Furthermore, the Raman spectra also show a 4  $\text{cm}^{-1}$  red shift for C=O bonds and a 9 and 12  $\text{cm}^{-1}$  red shift for both C-O bonds on methyl thioglycolate. C-H shifts are observed due to grafting of methyl thioglycolate. Overall, the elongation of the C-C aromatic bonds of styrene and the ester group of methyl thioglycolate bonds suggest that these are the interacting groups that lead to self-healing. Specifically, self-healing is likely to originate from either the  $\delta^+$   $\text{CH}_2$  or  $\delta^+$   $\text{CH}_3$  on either side of the ester accepting electron charge from the  $\delta^-$  centre of the benzene ring. As the benzene ring is more

stabilised, the  $\delta^+$  HC-CH aromatic bonds experience a weaker pull from the centre, hence the slightly longer bond length. Similar interactions to this are seen in nature that influence the secondary structure of proteins.<sup>33</sup>

The increased intermolecular interactions and phase compatibility can influence the polymer morphology evolution. As illustrated by small angle x-ray scattering (SAXS) in Figure 9a, the 2D SAXS image shows that SBS displays partial long-range order in one direction before modification. The 1D spectra for SBS also shows strong q peaks at  $\sqrt{3}$  and  $\sqrt{7}$  and a small hump at  $\sqrt{4}$ . This demonstrates that SBS has hexagonally arranged cylindrical styrene microdomains in a butadiene continuous phase.<sup>34</sup> In contrast, the 2D image of MGSBS clearly shows the solid and homogeneous intensity of the scattering, indicating a spherical morphology. From the 1D graph, there is a small secondary q-peak at  $\sqrt{3}$  suggesting that the morphology of MGSBS (98.5%) is misaligned spheres rather than spheres or cylinders due to the lack of q-peaks at  $\sqrt{2}$ ,  $\sqrt{4}$  and  $\sqrt{7}$ .

This transition from cylindrical morphology to the more disordered misaligned spherical morphology demonstrates a higher degree of mixing of the two polymer blocks or an increase in compatibility, which further supports the DMTA results in Figure 8.

The phase morphology of SBS before and after modification to MGSBS were observed by AFM and shown in Figure 9b. The SBS phase image shows hard styrene cylinders in dark and butadiene phase in light colour, showing a clear phase separation between the two phases. The height distribution graph for SBS shows two peaks for the two phases, Figure 9b. In comparison, for MGSBS, the cylindrical styrene phase has disappeared to show almost one uniform phase. The height distribution graph also shows only a single peak for one phase. The only existence of the styrene phase is the disordered arrangement of dark dots, small fragments that remain uncompatibilised by the ester. The few styrene spheres remaining give rise to the small q peak at  $\sqrt{3}$  in the SAXS 1D graphs.

Therefore, the vast majority of polystyrene block has been compatibilised by the chemical modification, resulting the two distinct phases with hexagonally arranged polystyrene cylinders

in a polybutadiene matrix transforming into a single disordered polymer phase with a small quantity of disordered polystyrene containing spheres.

The above characterisation results indicate that the mechanism of self-healing of MGSBS is as a result of an interaction between the  $\delta^-$  styrene ring and the  $\delta^+$  groups on either side of the ester of methyl thioglycolate. The transition to a more disordered phase morphology demonstrates the increased compatibility between the two phases to allow some phase mixing. Electrical breakdown of the elastomer occurs when a pinhole is formed due to the abrupt increase of the local strain and resultant mechanical rupture.<sup>1,35</sup> In the case of MGSBS, the intermolecular forces between the polymer chains have reunited the surfaces together to recover the breakdown strength and mechanical properties.

#### 4. Conclusions

A styrene-butadiene-styrene (SBS) was chemically modified using thiol-ene 'click' chemistry to graft methyl thioglycolate (MG) to the polymer backbone, where a high grafting ratio (98 mol%) of MGSBS were obtained via a one-step method. Detailed characterisation of the materials produced by this new approach provides the first report on the unexpected and remarkable self-healing capability of MGSBS to self-heal electrical and mechanical damage. A tensile strength recovery up to 25.4% and elongation at break recovery of 20.9% after three days was observed. MGSBS (68.3%) and MGSBS (98.5%) could be healed with no external stimuli and was simply performed by pushing two pieces together, yielding an instantaneous healing.

Characterisation indicated that the self-healing ability was caused by CH/ $\pi$  interactions between the methyl thioglycolate ester and the proton accepting aromatic system of styrene. At a low methyl thioglycolate grafting density, these interactions occurred intramolecularly and had a decreased chain entanglement when compared with SBS, resulting in a lower strength material without self-healing properties. At increased grafting levels, MGSBS displayed a strong self-healing ability and SAXS data indicated a change in morphology of SBS from hexagonally

arranged styrene cylinders to disordered spheres, showing a compatibilisation between the two blocks of SBS.

Grafting of MG group of 98% to SBS has reduced the Young's modulus by 94%, reduced the viscous loss by up to 80% at 300% elongation. Impedance spectroscopy measurements of MGSBS (98.5%) showed an increase in the relative permittivity of the elastomer from 2.8 to 11.4 at  $10^3$  Hz and maintained a low  $\tan \delta$  of  $9 \times 10^{-3}$ . These improvements led to improved actuation whereby MGSBS (98.5%) showed superior actuation performance compared to SBS, with an increase in area of 17% at an electric field of 250 kV cm<sup>-1</sup> and exhibited an actuation force of 0.12 N upon application of a 400 kV cm<sup>-1</sup> electric field, four times greater than SBS. The electrical breakdown for MGSBS (98.5%) recovered to 15% of its original breakdown strength after 24 hours of self-healing after breaking down at 200 kV cm<sup>-1</sup>. Overall, this work introduces a new class of self-healing dielectric elastomers using interactions typically seen in nature and results in a material which not only has excellent mechanical and electrical performances for actuation and energy generation applications but an increased longevity of life due to the unexpected self-healing nature.

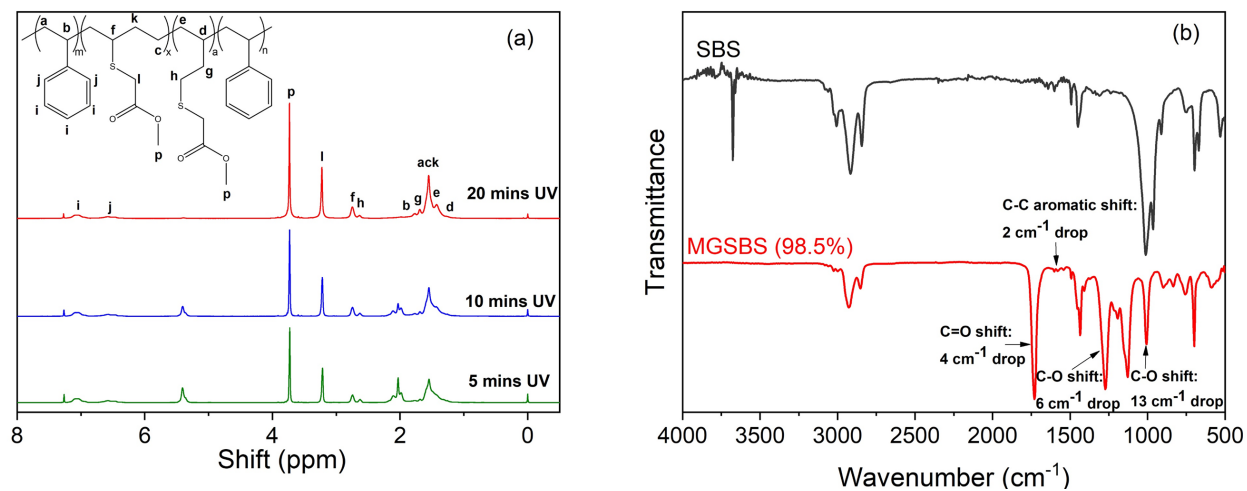


**Figure 1.** (a)  $^1\text{H}$  NMR of MGSBS: grafting 53.7 % / 5 mins UV, 68.3 % / 10 mins UV and 98.5 % / 20 mins UV; (b) FT-IR spectra of SBS and MGSBS (98.5%).

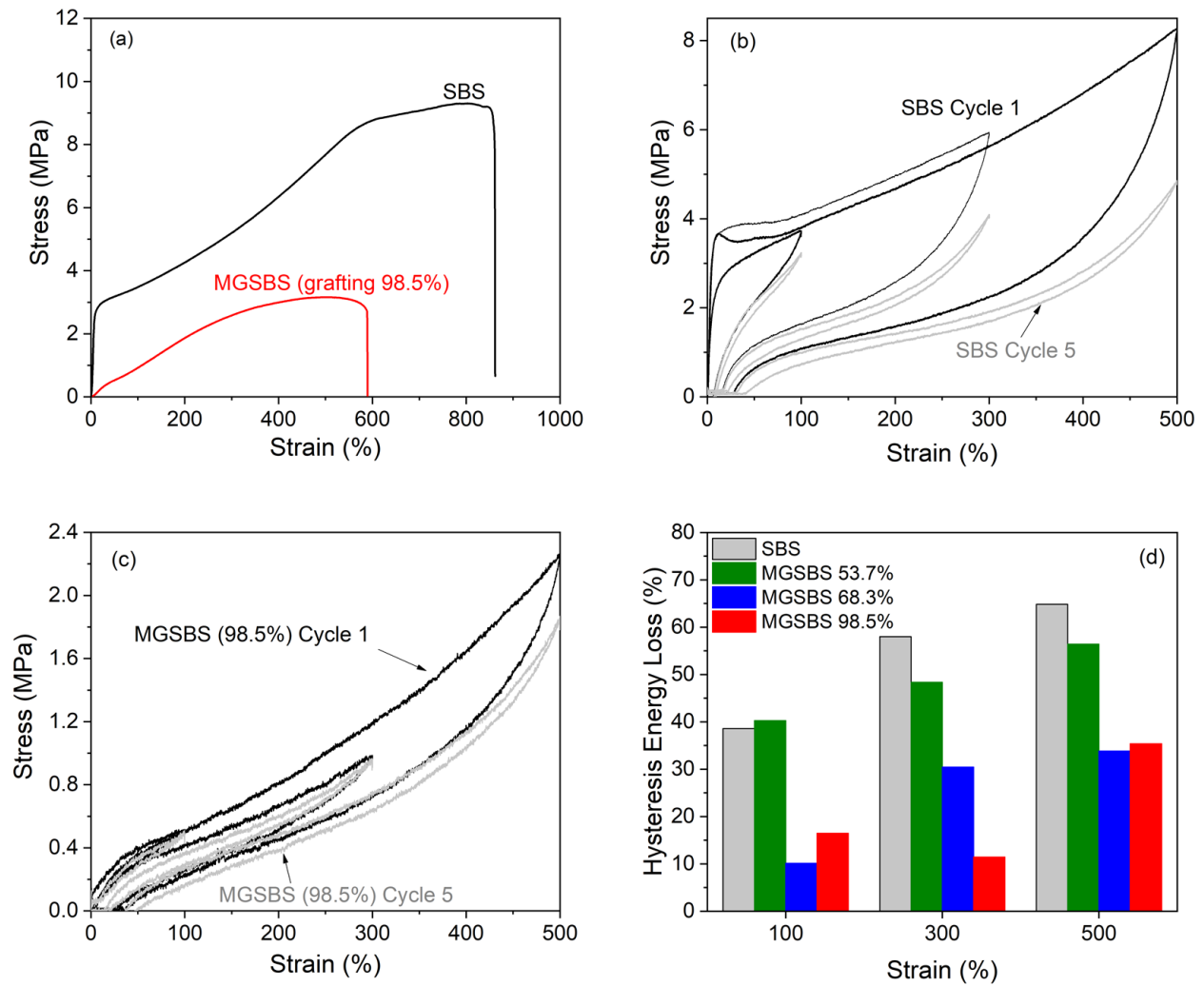


**Figure 2.** a) Stress-strain curves of SBS and MGSBS (98.5%); b) Stress-softening behaviour of SBS at different elongations after 1 cycle and 5 cycles. c) Stress-softening behaviour of MGSBS (98.5%) after 1 cycle and after 5 cycles. d) Hysteresis energy loss for SBS and MGSBS after 5 cycles.

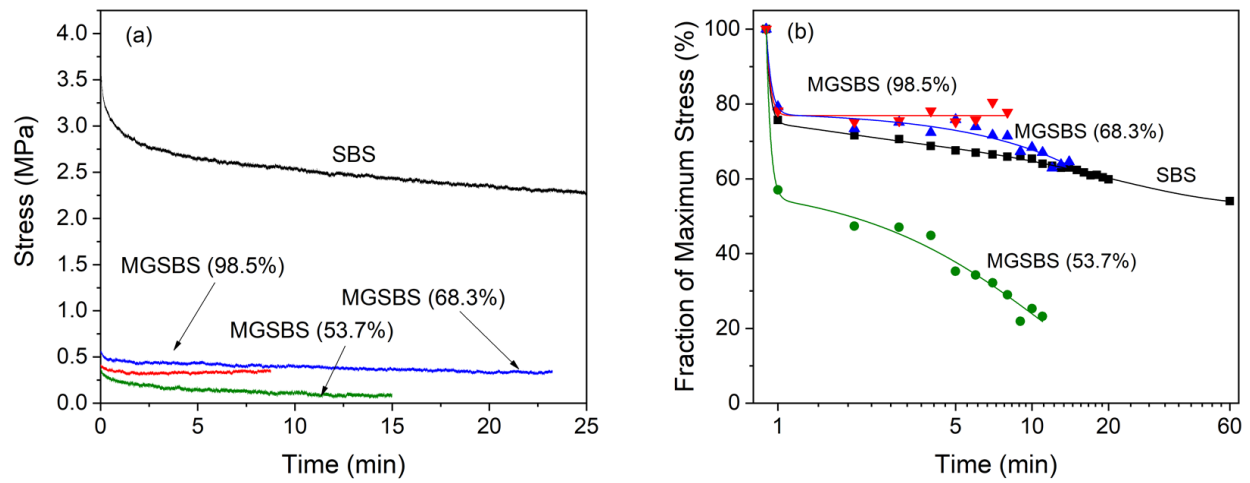


**Figure 3.** a) Stress vs time curve and b) Change in stress compared to initial stress of SBS and MGSBS at grafting ratios of 53.7%, 68.3% and 98.5%

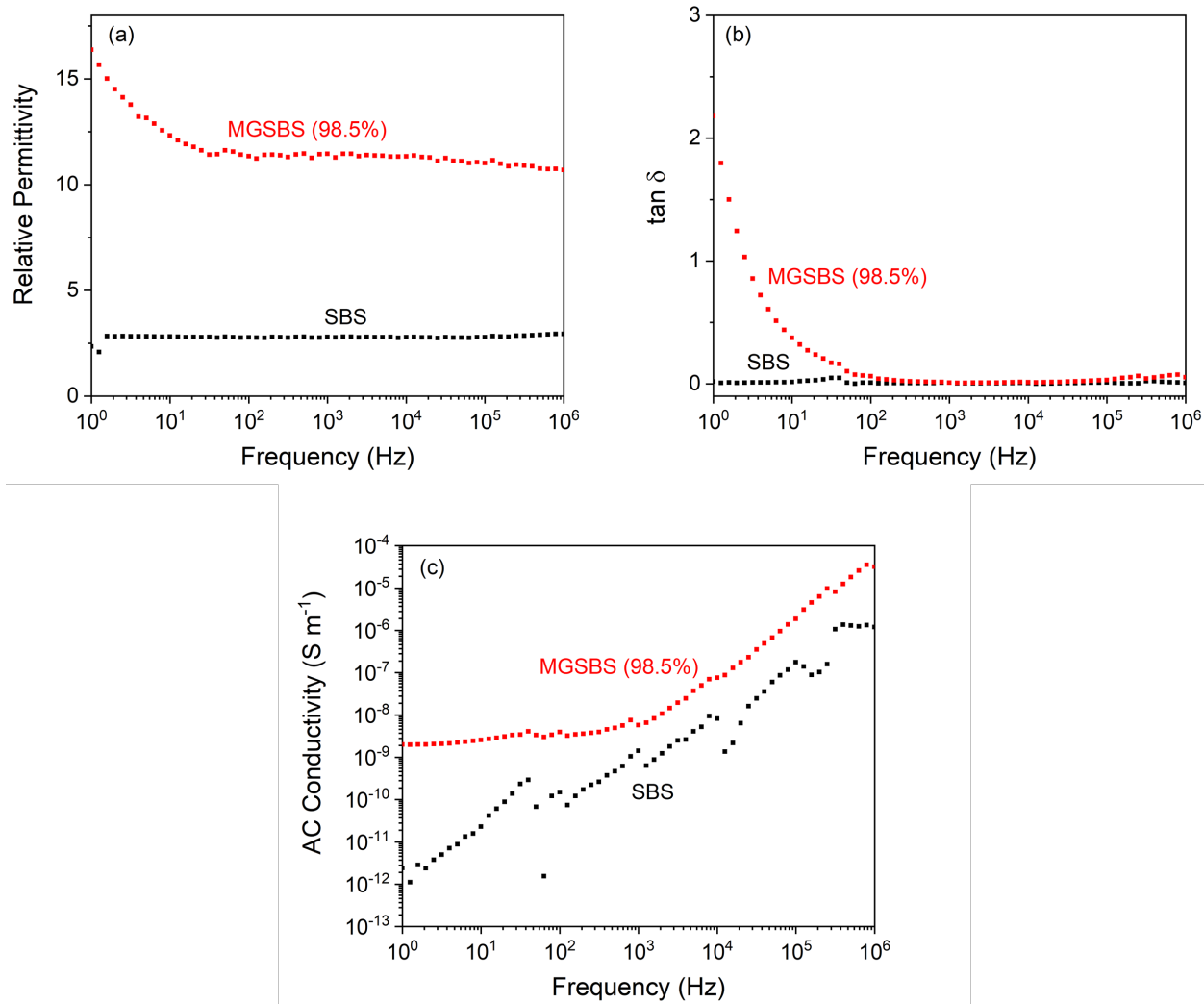


**Figure 4.** a) Relative permittivity, b)  $\tan \delta$ , c) AC conductivity of SBS and MGSBS (98.5%).



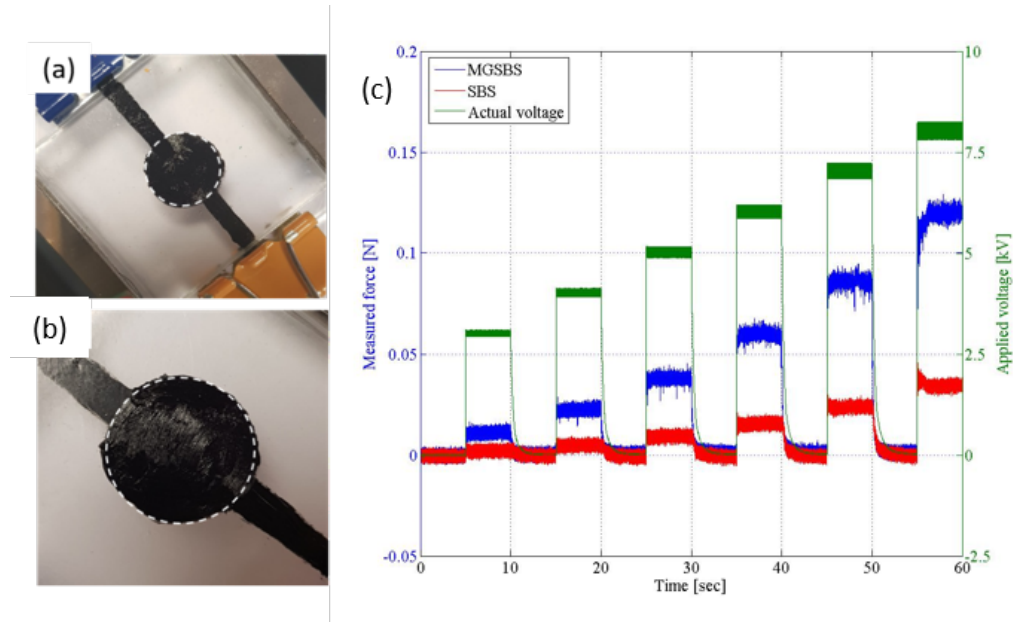


**Figure 5.** Actuation strain measurement in MGSBS at (a) 0 kV and (b) 5 kV shows the radial strain of approximately 13% and the areal strain of 17%. In comparison, the actuation strain measurement of SBS at 4 kV shows a radial strain of 1.2% and the areal strain of 1.4%. (Electric breakdown occurred immediately after voltage application in SBS at 5 kV; (c) Actuation force measurement in the MGSBS and SBS. At 8 kV, the MGSBS generates 0.12 N while the SBS generates 0.03 N.

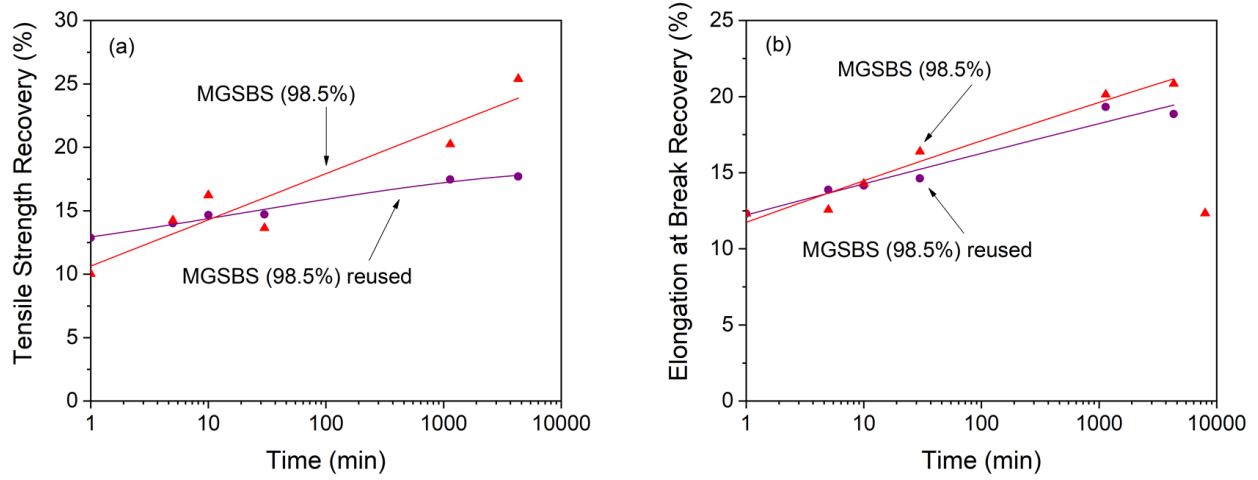


**Figure 6.** a) Tensile strength recovery; b) Elongation at break recovery of MGSBS (98.5%) native and reused.

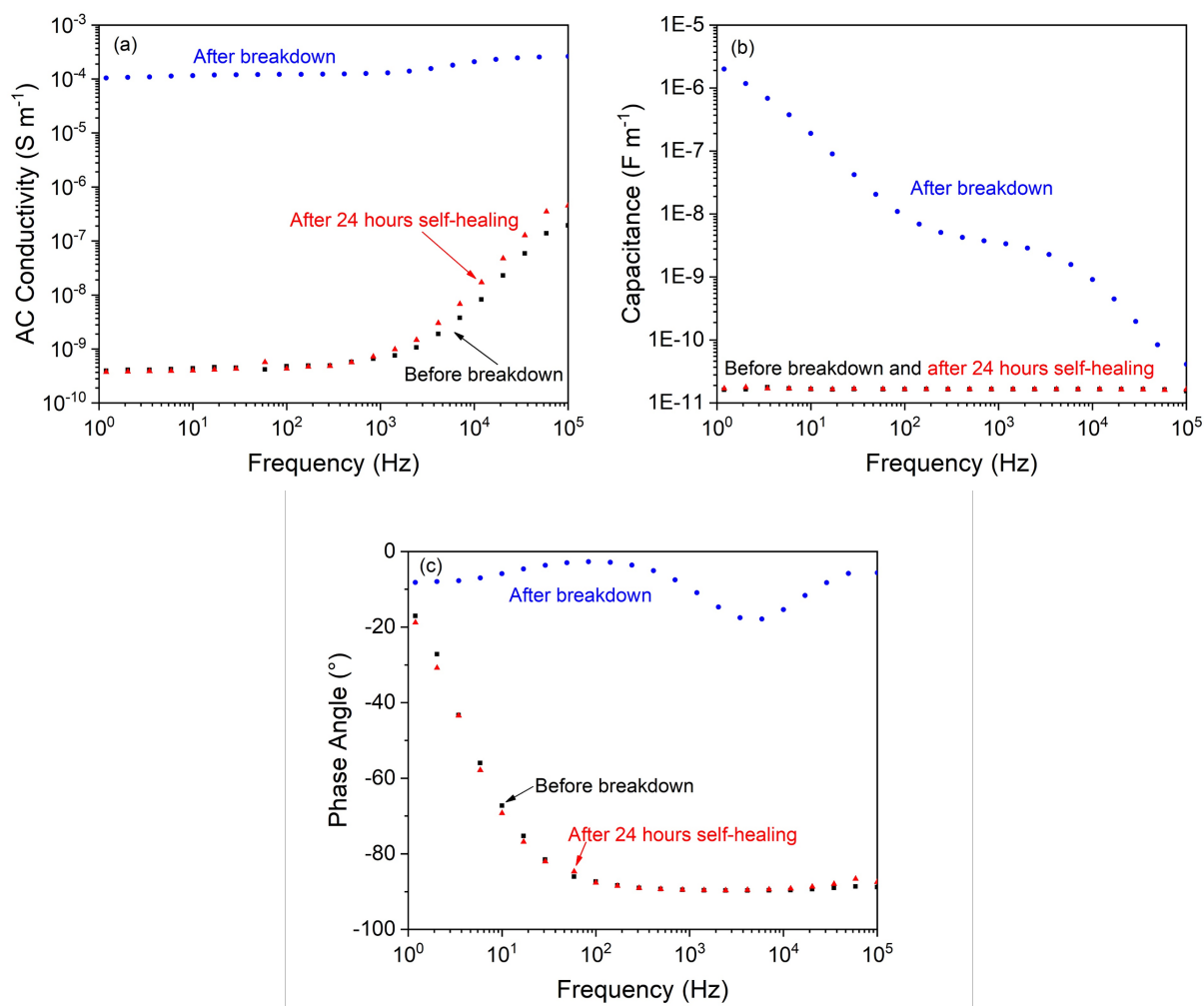


**Figure 7.** (a) AC conductivity (b) capacitance and (c) phase angle for MGSBS (98.5%) prior to breakdown, directly after breakdown and 24 hours after breakdown.

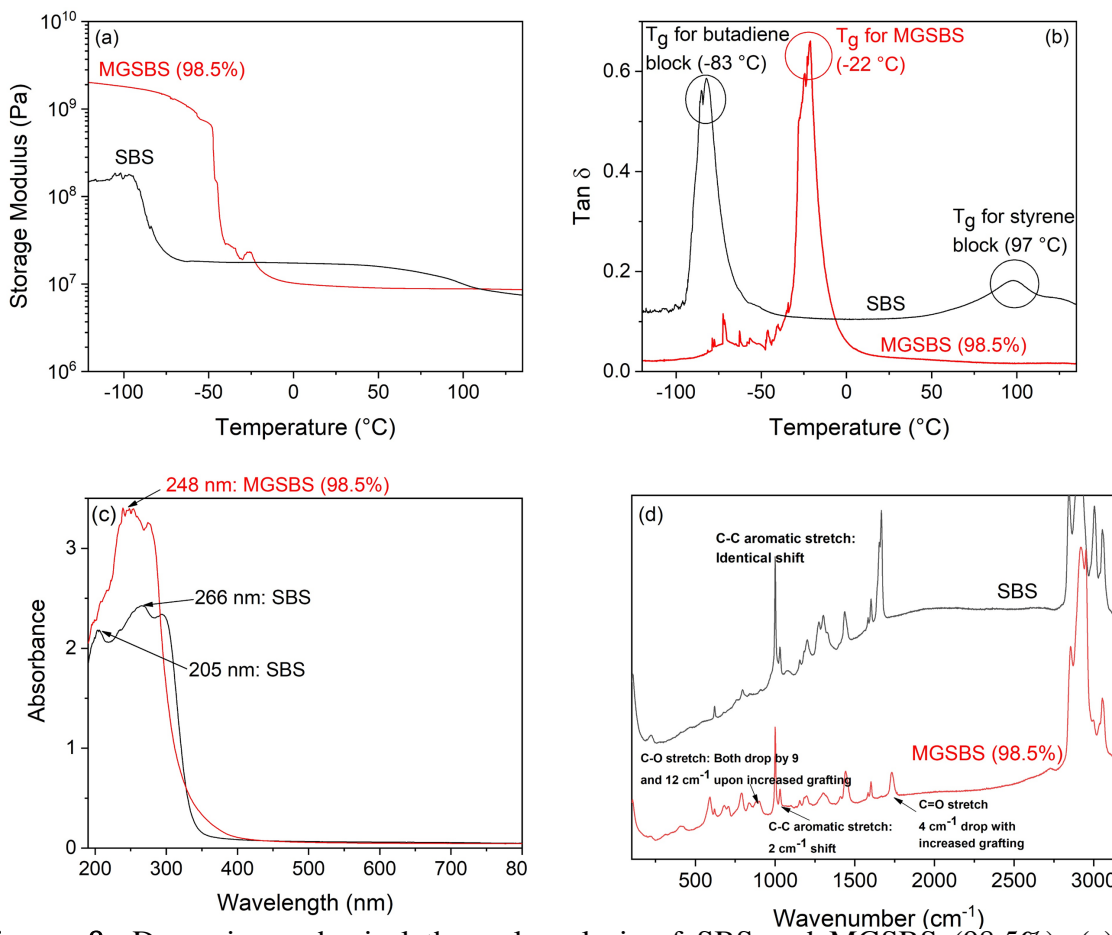


**Figure 8.** Dynamic mechanical thermal analysis of SBS and MGSBS (98.5%), (a) storage modulus, (b) mechanical tan  $\delta$  for the elastomers; (c) solid state UV-Vis spectra of SBS and MGSBS (98.5%) and (d) Raman spectra of SBS and MGSBS (98.5%).

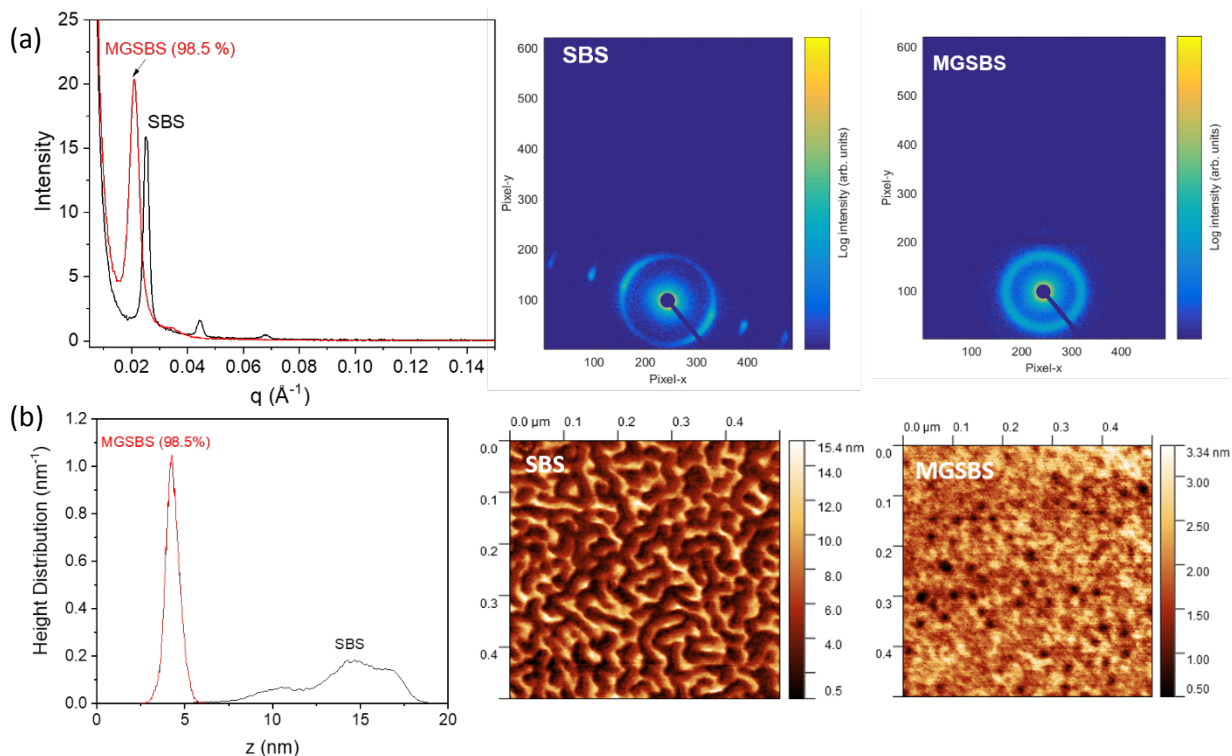


**Figure 9.** (a) 1D SAXS and 2D SAXS of SBS and MGSBS (98.5%); (b) AFM height distribution and phase morphologies of SBS and MGSBS (98.5%)

## ASSOCIATED CONTENT

### Supporting Information:

- 
- S1: Electrode configurations for (a) dielectric elastomer actuation in strain after pre-strain and setup for actuation strain measurement; (b) dielectric elastomer actuation in force prior to pre-strain and setup for actuation force measurement; (c) A 60 seconds voltage input sequence for actuation in strain.
- S2:  $^1\text{H}$  NMR of SBS.

- S3: Phase angle of SBS and MGSBS (98.5%).
- S4: a) tensile strength recovery; b) elongation at break recovery of MGSBS with grafting ratios of 68.3 and 98.5%.
- S5: a) tensile strength recovery; b) elongation at break recovery of MGSBS (98.5%) self-healed at 20 °C and 37 °C.
- S6: Polarisation – electric field response (a) as received material (b) 24 hours after breakdown and applied pressure up to 1 kV.
- S7: UV-Vis spectrum of SBS and MGSBS (98.5%) in solution state using DCM.

## AUTHOR INFORMATION

### **Corresponding Author**

Dr. Chaoying Wan

International Institute for Nanocomposites Manufacturing (IINM), WMG, University of Warwick, CV4 7AL, UK

Email: Chaoying.wan@warwick.ac.uk

### **Author Contributions**

The manuscript was written through contributions of all authors. All authors have given approval to the final version of the manuscript.

## ACKNOWLEDGMENT

CE thanks EPSRC and Jaguar Land Rover (UK) for funding this PhD studentship

## REFERENCES

- (1) Ellingford, C.; Bowen, C.; McNally, T.; Wan, C. Intrinsically Tuning the Electromechanical Properties of Elastomeric Dielectrics: A Chemistry Perspective. *Macromol. Rapid Commun.* **2018**, *39* (18), 1800340.
- (2) Brochu, P.; Pei, Q. Advances in Dielectric Elastomers for Actuators and Artificial Muscles. *Macromol. Rapid Commun.* **2010**, *31* (1), 10-36.
- (3) Kornbluh, R. D.; Pelrine, R.; Pei, Q.; Heydt, R.; Stanford, S.; Oh, S.; Eckerle, J., Electroelastomers: Applications of Dielectric Elastomer Transducers for Actuation, Generation, and Smart Structures. In *SPIE's 9th Annual International Symposium on Smart Structures and Materials*, SPIE: 2002; Vol. 4698, p 17.
- (4) Yang, D.; Ruan, M.; Huang, S.; Wu, Y.; Li, S.; Wang, H.; Ao, X.; Liang, Y.; Guo, W.; Zhang, L. Dopamine and Silane Functionalized Barium Titanate with Improved Electromechanical Properties for Silicone Dielectric Elastomers. *RSC Adv.* **2016**, *6* (93), 90172-90183.
- (5) Yang, D.; Ge, F.; Tian, M.; Ning, N.; Zhang, L.; Zhao, C.; Ito, K.; Nishi, T.; Wang, H.; Luan, Y. Dielectric Elastomer Actuator with Excellent Electromechanical Performance using Slide-ring Materials/Barium Titanate Composites. *J. Mater. Chem. A* **2015**, *3* (18), 9468-9479.
- (6) Yao, Z.; Song, Z.; Hao, H.; Yu, Z.; Cao, M.; Zhang, S.; Lanagan, M. T.; Liu, H. Homogeneous/Inhomogeneous-Structured Dielectrics and their Energy-Storage Performances. *Adv. Mater.* **2017**, *29* (20), 1601727.
- (7) Dang, Z.-M.; Zheng, M.-S.; Zha, J.-W. 1D/2D Carbon Nanomaterial-Polymer Dielectric Composites with High Permittivity for Power Energy Storage Applications. *Small* **2016**, *12* (13), 1688-1701.

- (8) Stoyanov, H.; Mc Carthy, D.; Kollosche, M.; Kofod, G. Dielectric Properties and Electric Breakdown Strength of a Subpercolative Composite of Carbon Black in Thermoplastic Copolymer. *Appl. Phys. Lett.* **2009**, *94* (23), 232905.
- (9) Zhao, H.; Xia, Y.-J.; Dang, Z.-M.; Zha, J.-W.; Hu, G.-H. Composition Dependence of Dielectric Properties, Elastic Modulus, and Electroactivity in (Carbon Black-BaTiO<sub>3</sub>)/Silicone Rubber Nanocomposites. *J. Appl. Polym. Sci.* **2013**, *127* (6), 4440-4445.
- (10) Nayak, S.; Chaki, T. K.; Khastgir, D. Development of Flexible Piezoelectric Poly(dimethylsiloxane)-BaTiO<sub>3</sub> Nanocomposites for Electrical Energy Harvesting. *Ind. Eng. Chem. Res.* **2014**, *53* (39), 14982-14992.
- (11) Wu, S.; Shao, M.; Burlingame, Q.; Chen, X.; Lin, M.; Xiao, K.; Zhang, Q. M. A High-K Ferroelectric Relaxor Terpolymer as a Gate Dielectric for Organic Thin Film Transistors. *Appl. Phys. Lett.* **2013**, *102* (1), 013301.
- (12) Thakur, V. K.; Tan, E. J.; Lin, M.-F.; Lee, P. S. Polystyrene Grafted Polyvinylidene fluoride Copolymers with High Capacitive Performance. *Polym. Chem.* **2011**, *2* (9), 2000-2009.
- (13) Putintsev, N. M.; Putintsev, D. N. The Molar Polarization and Refraction of Substances. *Russ. J. Phys. Chem.* **2006**, *80* (12), 1949-1952.
- (14) Racles, C.; Alexandru, M.; Bele, A.; Musteata, V. E.; Cazacu, M.; Opris, D. M. Chemical Modification of Polysiloxanes with Polar Pendant Groups by Co-hydrosilylation. *RSC Adv.* **2014**, *4* (71), 37620-37628.
- (15) Dunki, S. J.; Tress, M.; Kremer, F.; Ko, S. Y.; Nuesch, F. A.; Varganici, C.-D.; Racles, C.; Opris, D. M. Fine-tuning of the Dielectric Properties of Polysiloxanes by Chemical Modification. *RSC Adv.* **2015**, *5* (62), 50054-50062.



- (16) Dunki, S. J.; Nuesch, F. A.; Opris, D. M. Elastomers with Tunable Dielectric and Electromechanical Properties. *J. Mater. Chem. C* **2016**, *4* (44), 10545-10553.
- (17) Dunki, S. J.; Cuervo-Reyes, E.; Opris, D. M. A Facile Synthetic Strategy to Polysiloxanes Containing Sulfonyl Side Groups with High Dielectric Permittivity. *Polym. Chem.* **2017**, *8* (4), 715-724.
- (18) Zhang, C.; Wang, D.; He, J.; Liu, M.; Hu, G.-H.; Dang, Z.-M. Synthesis, Nanostructures and Dielectric Properties of Novel Liquid Crystalline Block Copolymers. *Polym. Chem.* **2014**, *5* (7), 2513-2520.
- (19) Zhang, C.; Wang, D.; He, J.; Liang, T.; Hu, G.-H.; Dang, Z.-M. Synthesis and Dielectric Properties of Novel Liquid Crystalline Triblock Copolymers with Cyanobiphenyl Moieties and Poly(n-butyl acrylate) Segments. *Polym. Adv. Technol.* **2014**, *25* (9), 920-926.
- (20) Huang, C.; Zhang, Q. M. Fully Functionalized High-Dielectric-Constant Nanophase Polymers with High Electromechanical Response. *Adv. Mater.* **2005**, *17* (9), 1153-1158.
- (21) Dünki, S. J.; Ko, Y. S.; Nüesch, F. A.; Opris, D. M. Self-Repairable, High Permittivity Dielectric Elastomers with Large Actuation Strains at Low Electric Fields. *Adv. Funct. Mater.* **2015**, *25* (16), 2467-2475.
- (22) Madsen, F. B.; Yu, L.; Skov, A. L. Self-Healing, High-Permittivity Silicone Dielectric Elastomer. *ACS Macro Lett.* **2016**, *5* (11), 1196-1200.
- (23) Wang, D.; Guo, J.; Zhang, H.; Cheng, B.; Shen, H.; Zhao, N.; Xu, J. Intelligent Rubber with Tailored Properties for Self-healing and Shape Memory. *J. Mater. Chem. A* **2015**, *3* (24), 12864-12872.

- (24) Li, C.-H.; Wang, C.; Keplinger, C.; Zuo, J.-L.; Jin, L.; Sun, Y.; Zheng, P.; Cao, Y.; Lissel, F.; Linder, C.; You, X.-Z.; Bao, Z. A Highly Stretchable Autonomous Self-healing Elastomer. *Nat. Chem.* **2016**, *8*, 618.
- (25) Sun, H.; Jiang, C.; Ning, N.; Zhang, L.; Tian, M.; Yuan, S. Homogeneous Dielectric Elastomers with Dramatically Improved Actuated Strain by Grafting Dipoles onto SBS using Thiol-ene Click Chemistry. *Polym. Chem.* **2016**, *7* (24), 4072-4080.
- (26) Lu, T.; Huang, J.; Jordi, C.; Kovacs, G.; Huang, R.; Clarke, D. R.; Suo, Z. Dielectric Elastomer Actuators under Equal-biaxial Forces, Uniaxial Forces, and Uniaxial Constraint of Stiff Fibers. *Soft Matter* **2012**, *8* (22), 6167-6173.
- (27) Rabuffi, M.; Picci, G. Status Quo and Future Prospects for Metallized Polypropylene Energy Storage Capacitors. *IEEE Trans. Plasma Sci.* **2002**, *30* (5), 1939-1942.
- (28) Jonscher, A. K. Low-frequency Dispersion in Carrier-dominated Dielectri. *Philos. Mag. B* **1978**, *38* (6), 587-601.
- (29) Yu, L.; Madsen, F. B.; Skov, A. L. Degradation Patterns of Silicone-based Dielectric Elastomers in Electrical Fields. *Int. J. Smart Nano Mater.* **2017**, 1-16.
- (30) Almond, D. P.; Bowen, C. R. An Explanation of the Photoinduced Giant Dielectric Constant of Lead Halide Perovskite Solar Cells. *J. Phys. Chem. Lett.* **2015**, *6* (9), 1736-1740.
- (31) Sobczyk, L.; Grabowski, S. J.; Krygowski, T. M. Interrelation between H-Bond and Pi-Electron Delocalization. *Chem. Rev.* **2005**, *105* (10), 3513-3560.
- (32) Beavan, S. W.; Phillips, D. Mechanistic Studies on the Photo-oxidation of Commercial Poly(butadiene). *Eur. Polym. J.* **1974**, *10* (7), 593-603.

- (33) Suresh, C. H.; Neetha, M.; Vijayalakshmi, K. P.; Renjumon, G.; Mathew, J. M. Typical Aromatic Noncovalent Interactions in Proteins: A Theoretical Study using Phenylalanine. *J. Comput. Chem.* **2009**, *30* (9), 1392-1404.
- (34) Morrison, F. A.; Winter, H. H. The Effect of Unidirectional Shear on the Structure of Triblock Copolymers. I. Polystyrene-polybutadiene-polystyrene. *Macromolecules* **1989**, *22* (9), 3533-3540.
- (35) Moscardo, M.; Zhao, X.; Suo, Z.; Lapusta, Y. On Designing Dielectric Elastomer Actuators. *J. Appl. Phys.* **2008**, *104* (9), 093503.